ACS OMEGA

http://pubs.acs.org/journal/acsodf

Article

EA-Directing Formamidinium-Based Perovskite Microwires with A-Site Doping

Shan Xu,[⊥] Xue Ding,[⊥] Huafeng Shi, Xinhai Zhang, Xiaowei Sun, Ning Ji, Xiaoli Zhang,* and Zhaoyu Zhang*

Cite This: *ACS Omega* 2021, 6, 7157−7164

Read Online

ACCESS | Metrics & More | Article Recommendations | Supporting Information

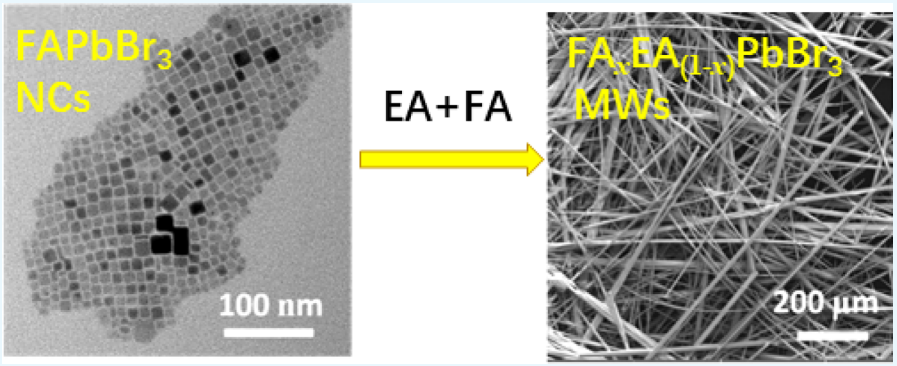

ABSTRACT: One recent development to improve optoelectronic properties of perovskites is to use a larger cation for multication engineering. The chain-like ethylammonium (EA) $[(C_2H_5)NH_3]^+$ cation is more likely to form a one-dimensional perovskite structure; however, there is no remarkable evidence in this connection. Therefore, in this work, for the first time, the EA cation as an alternative cation was introduced into $FAPbBr_3$ cubic crystals to explore the stabilities and optoelectronic properties of mixed $FA_xEA_{(1-x)}PbBr_3$ perovskites. The results indicate that replacing FA with EA is a more effective way to realize band gap tuning and morphology transformation between the cubic shape and microwires. The tuned band gap of perovskite is due to the variation of Pb−Br−Pb angles induced by the insertion of the larger EA cation. We highlight that this work provides new physical insights into the correlation between the engineering of organic cations and the formation of perovskite microwires and the tunable band gap. This observation will help us to find new ways to grow perovskite microwires and subsequently study the optoelectronic performance of low-dimensional perovskites devices.

1. INTRODUCTION

Metal halide perovskites have recently become a scientific spotlight in the field of photonics and optoelectronics. The great success of perovskite as a new generation of semiconducting materials has been widely witnessed in photovoltaics, light-emitting diodes (LEDs), transistors, photodetectors, and lasers.[1−8] With general chemical stoichiometry ABX_3, perovskite is typically composed of cation A, metal cation B, and halide anion X. The wide feasibility of the combination of different cations and halide anions in perovskites has promoted large possibilities in compositional engineering for different applications.[9−14] There are several synthesis strategies for organic−inorganic hybrid perovskite nanomaterials, including the template method, hot injection method, ligand-assisted reprecipitation strategy, chemical vapor deposition method, microfluidic reactor method, ultrasound synthesis, and mechanical ball milling method.[15−19] In perovskite materials, the A-site cation, such as methylammonium (CH_3NH_3, MA), formamidinium ($HC(NH_2)_2$, FA), or caesium (Cs), as an important effective component, plays a key role in tuning the crystal structure and optical and electronic properties. For example, Br vacancies and interstitials have much lower formation energies and higher density in MA cation-based perovskite than FA-based crystals, while a higher rotation barrier and stronger H-bonding between the organic cation and Br are in the latter case.[20] As certified in density functional theory (DFT), incorporating organic cations with the appropriate structure, shape, and strong H-bonding capabilities in perovskite crystal facilitates the suppression of ion migration and charge accumulation and

Received: January 12, 2021
Accepted: March 1, 2021
Published: March 8, 2021

https://dx.doi.org/10.1021/acsomega.1c00213
ACS Omega 2021, 6, 7157−7164

further improves the performance of perovskite optoelectronic devices.[21,22]

Hybrid perovskites with mixed cations have demonstrated tremendous advances in photovoltaics and LEDs, with greatly enhanced performance and stability. For example, Zhang et al. synthesized mixed cation perovskite nanocrystals based on $FA_{(1-x)}Cs_xPbBr_3$, and the corresponding LEDs with the optimized composition (x = 0.2) exhibited encouraging performance with the highest luminance of 55,005 cd m^{-2} and a current density above 10 cd A^{-1}.[8] Mixed cation-based perovskites demonstrate that compositional modulation could boost the crystallinity and conversion efficiency. A small amount of the MA cation is sufficient to realize a perfect crystallinity in FA-based perovskite.[23] The Cs cation with a smaller ionic radius is found to be effective in assisting the crystallization of the black phase of FA perovskite with photostability and thermal stability due to entropic stabilization[24] and promoting the efficiency of solar cells.[25,26]

One recent development to improve optoelectronic properties of perovskites is to use a larger cation for polycationic engineering, such as the ethylammonium (EA) $[(C_2H_5)NH_3]^+$ cation. It has been widely reported for the research and development of devices with EA added to perovskites,[27−31] especially for the mixture of MA cations and its higher analog EA cations, which provide a versatile tool to tune the structural as well as optoelectronic properties of perovskite. Moreover, EA has a larger ionic radius (2.74 Å) than that of MA (2.17 Å), and the addition of EA can be expected to improve stability from the viewpoint of calculations and tolerance factor[32] and the thermal stability and crystallinity due to fewer defects during surface coating.[33] The reported A-site cation effect on the optoelectronic and photonic device is primarily based on polycrystalline perovskite or thin films, while the low-dimensional perovskite nanostructure with a mixed cation is rarely studied. The perovskite with reduced dimensionality has attracted much attention due to the quantum confinement effects, providing a platform to well modulate exciton−photon interaction and exciton binding energy,[34−36] offering great support for advancing the fundamental understanding of perovskites as well as technological applications.[37] Therefore, it is important to actively get into developing ways to achieve controllable and reproducible production of low-dimensional perovskites based on mixed cations and study the structure (morphology)−property relationship underlying it.

As one of the basic building blocks, perovskites nanowires (NWs) or microwires (MWs) have been widely investigated for their tunable band gaps, anisotropic optoelectronic properties, and outstanding efficiency. As is well-known, the dimensionality and morphology of perovskite crystallites are strikingly influenced by various factors, such as solvents, surface ligands, additives, reaction temperatures, and time. Under most circumstances, cubic perovskite crystallites with isotropic shapes have been observed. For perovskite nanowires or nanorods, in principle, there should be a crystallographic driving force for anisotropic growth. The chain-like EA organic cation is more likely to a form a one-dimensional perovskite structure; however, there is no remarkable evidence in this connection. Therefore, in this work, for the first time, the EA cation as an alternative cation was introduced into $FAPbBr_3$ cubic crystals to explore the stabilities and optoelectronic properties of mixed $FA_xEA_{(1-x)}PbBr_3$ perovskites. The results indicate that replacing FA with EA is a more effective way to realize band gap tuning and morphology transformation between the cubic shape and microwires. The growth process and physicochemical and optoelectronic properties have been systematically surveyed. We highlight that this work provides new physical insights into the correlation between the engineering of organic cations and the formation of perovskite microwires and a tunable band gap. This observation will help us to find new ways to grow perovskite microwires and subsequently study the optoelectronic performance of low-dimensional perovskites devices.

2. METHOD

2.1. Materials. Formamidinium bromide (FABr), ethylammonium bromide (EABr), and lead bromide ($PbBr_2$) were ordered from Sigma. Dimethyl formamide (DMF) and toluene were purchased from Alfa-Aesar.

2.2. Synthesis of Perovskite Microwires. The synthesis of perovskite microwires was carried out at room temperature using the ligand-assisted reprecipitation technique. First, concentration-fixed solutions of $PbBr_2$ (0.5 M), EABr (1 M), and FABr (1 M) dissolved in DMF were prepared. Calculated amounts of FABr, EABr, and $PbBr_2$ solutions as well as certain additives were injected into a clean bottle to obtain the precursor at room temperature. The details are given in Table S1. Then, the green solution was synthesized when the prepared precursor was dropwise added into 10 mL of toluene followed by the slow growth of perovskite microwires with time. The resulting perovskite microwires were collected for further analysis.

2.3. Characterization. The steady-state PL spectra were measured by using a spectrometer (SP2300) with a CCD detector (PIX400BRX) under excitation by a He−Cd gas laser with a wavelength of 325 nm. The lifetime of samples was measured by a time-correlated single-photo counting system under excitation of a 375 nm pulse laser (∼40 ps). X-ray diffraction analysis was carried out with an XRD Bruker D8 Advance, while the morphological images were detected with FESEM (field-emission scanning electron microscopy; JEOL JSM-7600F) and TEM (transmission electron microscopy; Tecnai F30 microscope).

3. RESULTS AND DISCUSSION

The colloidal method, widely and successfully applied on the synthesis of perovskite nanocrystals, has been sequentially introduced into the fabrication of perovskite nanowires. Colloidal synthesis was based on an antisolvent precipitation method.[38,39] In detail, as shown in Figure 1, $PbBr_2$, FABr, and/or EABr were dissolved in a polar solvent DMF and the precursor was added into a solvent with lower polarity such as toluene. The addition of a single FABr-formed precursor into toluene promotes the production of common $FAPbBr_3$ nanocrystals with a cubic shape (Figure 1a), while the joining of the EA alternative cation directs the evolution of perovskite microwires after a prolonged reaction time (Figure 1b). The photographs of perovskite evolution are shown in Figure S1, and the SEM images of crystal transformation at different times are shown in Figure S2.

To gain insights into the role of the additive EA cation on the perovskite crystal structure, the EA-directing morphology transformation is further evidenced by high-resolution SEM in Figure 2. The clear $FAPbBr_3$ solution shows a green color, and the size of the nanocrystal is about 10 nm in cubic shape (Figure 2a−c). Interestingly, mixed cation perovskite

https://dx.doi.org/10.1021/acsomega.1c00213
ACS Omega 2021, 6, 7157−7164

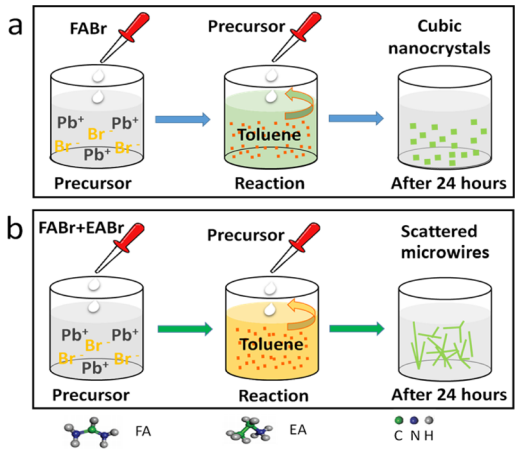

Figure 1. Schematic diagram of the synthesis process of perovskite (a) $FAPbBr_3$ nanocrystals and (b) $FA_xEA_{(1-x)}PbBr_3$ microwires.

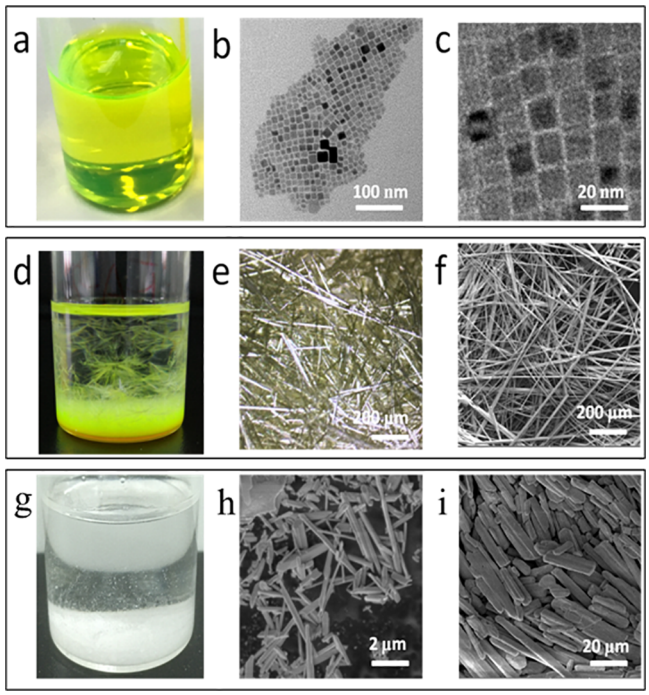

Figure 2. (a) Photograph and (b, c) TEM images of $FAPbBr_3$. (d) Photograph, (e) optical microscopy images, and (f) SEM images of $FA_xEA_{(1-x)}PbBr_3$ (x = 0.75) microwires. (g) Photograph and (h, i) SEM images of $EAPbBr_3$ nanorods.

$FA_xEA_{(1-x)}PbBr_3$ (x = 0.25−0.75) exhibits uniform microwires. Take x = 0.75 for example; the modulation of the EA cation in the A-site of perovskite promotes the generation of eye-catching scattered microwires in solution (Figure 2d), and the length of scattered microwires is up to a centimeter level (Figure 2e,f). For comparison, $EAPbBr_3$ solution presents white precipitation, and $EAPbBr_3$ nanorods with mean diameters of 600 nm and lengths of up to 50 μm were fabricated during the solution-mediated crystallization process (Figure 2g−i). The as-prepared $EAPbBr_3$ nanorods tend to form bundles in colloidal solution and settle at the bottom of the sample vial owing to their larger mass. Moreover, the aggregated microwires or nanorods are also attributed to the strong hydrophobic interactions between the ligand molecules. More evidence about the structure is presented below in the discussion on X-ray diffraction (XRD) and transition electron microscopy (TEM).

The growth progress of perovskite microwires is recorded at different times, and the corresponding images are observed by SEM (see the Supporting Information, Figure S1). We take $FA_xEA_{(1-x)}PbBr_3$ (x = 0.75) microwires as an example for further analysis. Optical microscopy was performed to confirm the crystallization of the perovskite microwires. As shown in Figure 3a, the perovskite microwires are uniformly spread, and the image of the thickness profile shows a uniform green color, indicating that the perovskite microwires are comparable in diameter and thickness. The detailed size distribution of microwires is calculated in Figure 3b, and histograms clearly signify the average diameter of microwires of 3 μm. The high-resolution TEM analysis in Figure 3c makes it clear that the prepared EA-directing perovskite microwires are highly crystalline, and the Fourier transform TEM images in Figure 3d confirm the microwires with highly oriented crystal planes. In general, perovskite nanocrystals tend to grow uniformly along the three major crystallographic directors, crystallizing in an isotropic cubic structure. Furthermore, the microwire growth was generally attributed to the directional effect of DMF where an internal complex with the methylamine group was formed during the crystallization process.[40−42] Compared to $FAPbBr_3$ nanocrystals, the only thing that has changed in the contrastive experiment is the addition of the EA cation. Surprisingly, in this work, the foreign EA cation facilitates the competition among the growth fronts from neighboring nucleation centers, which is more likely the crystallographic driving force for the highly anisotropic growth of perovskite microwires. Therefore, we can conclude that the mixed cation perovskite microwires spontaneously grow along the in-plane direction due to the EA cation.

The minor alterations of the applied processing parameters may lead to diverse nucleation and crystal growth of perovskites. To identify the effects of incorporation of the EA cation on the crystallization of the as-prepared $FA_xEA_{(1-x)}PbBr_3$ perovskites, X-ray diffraction (XRD) was employed on a series of perovskite samples, which were deposited on a glass substrate. As shown in Figure 4a, the standard perovskite crystal phase was detected throughout the entire composition range from x = 1 to x = 0.25. The zoomed diffraction patterns that peaked around 15° (001) and 30° (002) planes are shown in Figure 4b, which displayed an obvious peak shift toward smaller degrees. The radius of EA (2.74 Å) is slightly larger than FA (2.70 Å), which makes EA a suitable candidate for multication perovskite that has potential for beneficial and unexpected properties. The decreased diffraction angles with increasing the amount of EA cation doping are attributed to an expansion of the crystal lattice by insertion of the larger EA cations.[43,44] The continuous shift of the perovskite $FA_xEA_{(1-x)}PbBr_3$ phase indicates the doping of the EA and FA organic cation in the same lattice. Thus, EA is definitely going into the core perovskite. When the ratio of FA/EA was below 1:1 (x = 0.5, 0.3, and 0.25), additional diffraction peaks assigned to $EAPbBr_3$,[45] such as peaks at ∼15.8° and 30.9°, appeared in the XRD patterns. As the EA cation continues to increase, additional diffraction peaks are correspondingly strengthened, implying a smooth phase transition from $FA_xEA_{(1-x)}PbBr_3$ to mixed perovskites. That is, an excessive addition of EA leads to phase separation and a decrease in crystallization. The XRD patterns of representative $FA_xEA_{(1-x)}PbBr_3$ (x = 0.75) microwires containing a series of

https://dx.doi.org/10.1021/acsomega.1c00213
ACS Omega 2021, 6, 7157−7164

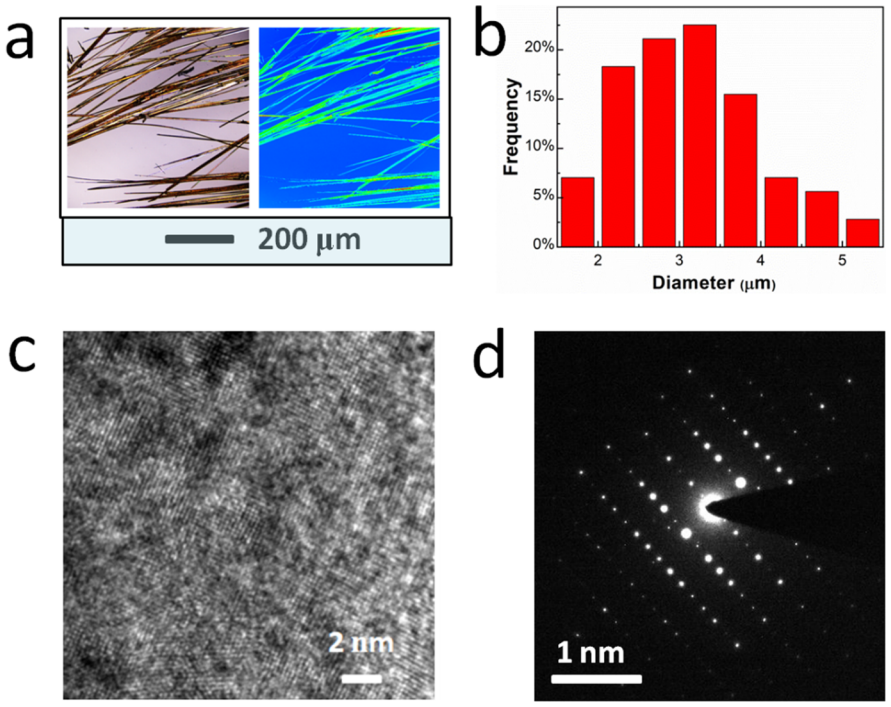

Figure 3. (a) Optical microscopy images of perovskite $FA_xEA_{(1-x)}PbBr_3$ (x = 0.75) microwires. (b) Size distribution histograms of microwires. (c) High-resolution TEM images. (d) Fourier transform TEM images.

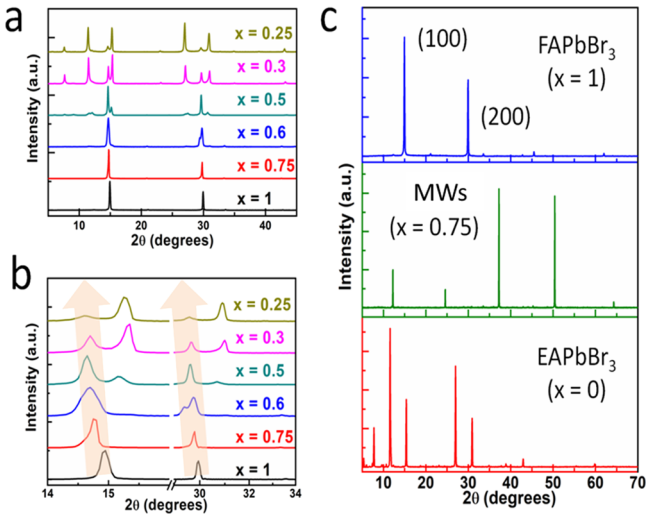

Figure 4. (a) XRD diffraction patterns of mixed cation $FA_xEA_{(1-x)}PbBr_3$. (b) Zoomed diffraction patterns peaked around 15° (001) and 30° (002) planes. (c) XRD diffraction patterns of perovskites $FAPbBr_3$, mixed cation $FA_{0.75}EA_{0.25}PbBr_3$, and $EAPbBr_3$.

well-defined periodically distributed diffraction peaks, with a preferential orientation toward the (00l) (l = 1, 2, 3, and 4) planes, confirm that the EA-directing perovskite microwires are highly oriented, with the c axis perpendicular to the substrate plane.

The images of obtained perovskite microwires are shown in Figure 5 under ambient light and UV light. The representative microwire selected for further analysis is $FA_xEA_{(1-x)}PbBr_3$ (x = 0.75), which shows a yellowish color in the air and green light emitting under UV excitation. The microwires collected directly from solution are stuck together and present bundle shapes, with a centimeter-sized length and a diameter above ~3 μm (Figure 5a,b). The photoluminescence (PL) and UV−vis absorption of freshly synthesized $FA_xEA_{(1-x)}PbBr_3$ are shown in Figure 5c. The as-synthesized $FAPbBr_3$ nanocrystals showed an absorption band at ~550 nm and a narrow emission at 552 nm with 20 nm full width at half-maximum (FWHM). The main absorption and emission maxima blue-shift upon increasing the concentration of the EA cation, and the detailed photophysical properties of all samples are summarized in Table S2. The band gap of $FA_xEA_{(1-x)}PbBr_3$ slightly increases with x from 1.0 to 0.25. As mentioned in empirical Vegard's law,[46] the band gap in the semiconductor is approximately a linear function of the lattice parameter, and a linear relationship also exists between the band gap and composition. In this work, the regular variation in the crystal lattice indicates the potential increased band gap of perovskites. On the other hand, it has been reported that the optical band gap of perovskite can be affected by the size of the organic ammonium cation due to either variation in the Pb−Br−Pb angle or formation of large barriers between semiconductor layers.[47] Therefore, we can estimate that the introduction of the EA cation resulting in the c axis distortion of the Pb−Br−Pb bond angles plays a great role in tuning the band gap.

When introducing more EA cations in $FA_xEA_{(1-x)}PbBr_3$ (x = 0.6 and 0.5), there is a weak emission peak around 470 nm, which overlaps with $EAPbBr_3$ (see Figure S3). The $EAPbBr_3$ nanowires show blue emission that peaked at 450 nm with FWHM above 50 nm. When EA doping is too much (x = 0.3 and 0.25), we observe blue emission features in the PL studies with a big tailing at a longer wavelength, indicating that EA may not completely go into the $FA_xEA_{(1-x)}PbBr_3$ perovskite structure when there is excess EA cation. The photoluminescence quantum yields (QYs) of $FAPbBr_3$ and $EAPbBr_3$ NCs are 82 and 5%, respectively, and the QYs of other perovskites $FA_xEA_{(1-x)}PbBr_3$ with mixed cations lie between these two results. Due to the differences in the cation types, the

https://dx.doi.org/10.1021/acsomega.1c00213
ACS Omega 2021, 6, 7157−7164

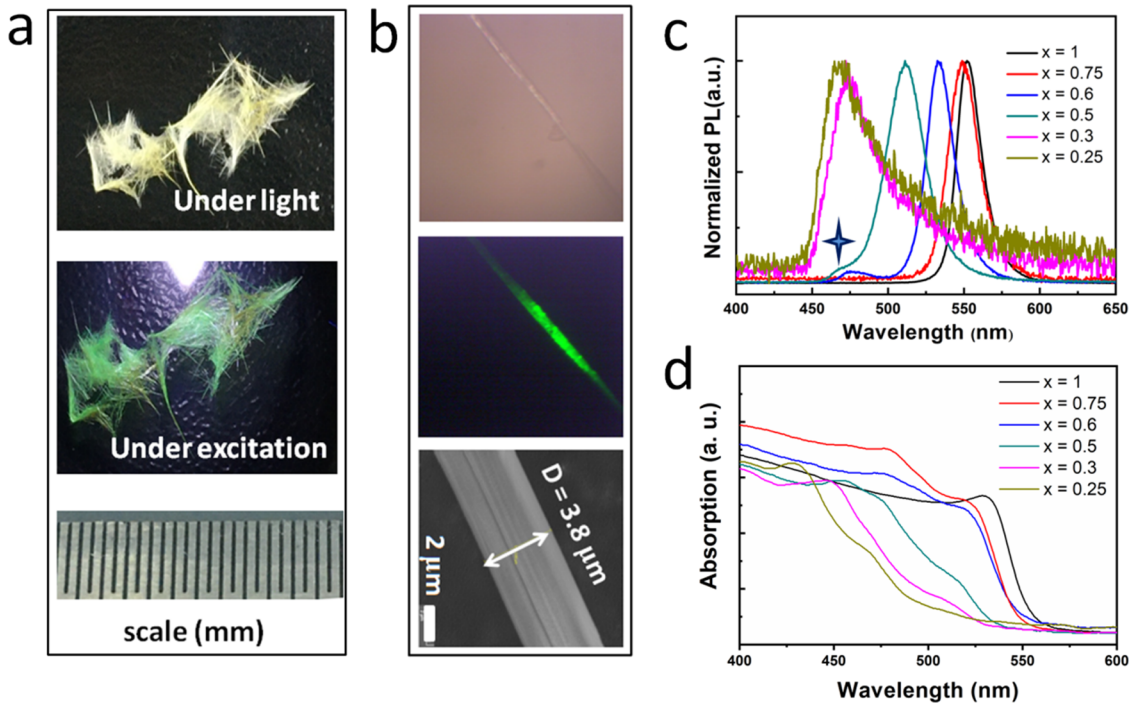

Figure 5. (a) Photographs of collected perovskite microwires under natural light and UV light. (b) Photographs of representative single microwires under the micro area test and its surface SEM image. (c) PL spectra and (d) absorption spectra of samples.

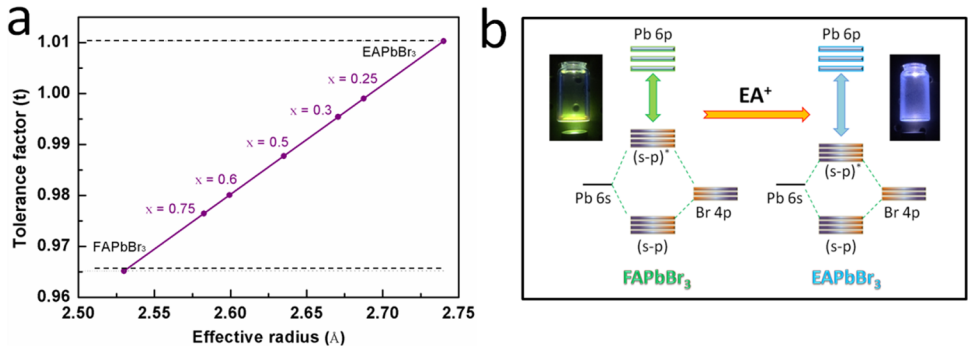

Figure 6. (a) Tolerance factor of perovskite $FA_xEA_{(1-x)}PbBr_3$. (b) Schematic representation of variation of energy levels from $FAPbBr_3$ in Pb 6p and Pb 6s−Br 4p orbitals on insertion of the EA cation.

interaction of EA and FA will be different toward core geometry as the number of N−H bonds varies in these cations. Therefore, for excessive doping, the low quantum yields are probably a result of the distortion of the structure and creation of traps.

To maintain symmetry and a stable crystal structure, the tolerance factor t of metal-halide perovskite ABX_3 should be close to 1, which is determined from the equation as below

$$t = \frac{r_A + r_X}{\sqrt{2}(r_B + r_X)} \quad (1)$$

where r_A, r_B, and r_X are the perovskite constituents' ionic radii, such as organic cation A, metal cation B, and halide anion X. In this work, the radii of organic FA^+ and EA^+, metal Pb^+, and halide Br^- are 2.53, 2.74, 1.33, and 1.96 Å, respectively, and the tolerance factor of mixed cation perovskite is calculated based on these effective ionic radii; the details are summarized in Table S3. The variation of t with the doping proportion is presented in Figure 6a, and we note that $EAPbBr_3$ has a tolerance factor exceeding 1. Therefore, as confirmed in the discussion above, the excess incorporation of the EA cation in perovskite resulted in the tilting of $PbBr_6$ octahedra, lowered symmetry, and then the degraded crystal quality and optical performance.

The performance of mixed cation perovskite is affected by the size of the organic ammonium cation via the variation of the Pb−Br−Pb angle. To have a deeper insight into this mixed cation structure, the schematic energy levels of $FAPbBr_3$ and $EAPbBr_3$ are shown in Figure 6b, which presents the energy levels of Pb 6s and (Pb 6s−Br 4p)* orbitals. As indicated, the insertion of a larger EA cation is proposed to increase the distance between Pb atoms and then the Pb−Br bond lengths, resulting in the decreased orbital overlap between the Pb 6s and Br 4p orbitals. The band gap is defined between the Pb 6s−Br 4p hybridized orbitals and Pb 6s levels,[45] and deservedly, the decreased Pb 6s−Br 4p orbital overlap will definitely increase the final band gaps of perovskite.

https://dx.doi.org/10.1021/acsomega.1c00213
ACS Omega 2021, 6, 7157−7164

4. CONCLUSIONS

In this work, we report for the first time the room-temperature colloidal synthesis of EA-directing perovskite microwires. Mixed cation perovskite shows green emission at 552 nm and also demonstrates the tunability of this emission from green to blue (471 nm) by varying the ratio of EA and FA cations. The EA-directing perovskite microwires provide a platform to fabricate low-dimensional perovskite with tuned optoelectronic properties and their use in optoelectronic devices. Mixed cation perovskite induced tuned band gaps due to the variation of the Pb−Br−Pb angle via incorporation of the larger EA cation. The excess EA insertion in the organic cation in perovskite results in phase separation and degraded crystal and performance. Therefore, it is critical to have fine control over the nucleation and crystal growth of perovskites.

■ ASSOCIATED CONTENT

Supporting Information

The Supporting Information is available free of charge at https://pubs.acs.org/doi/10.1021/acsomega.1c00213.

The transformation of the perovskite crystal to microwires (Figure S1a), the growth of perovskite microwires at different times (Figure S1b), SEM of crystal transformation at different times (Figure S2), the PL spectra of $EAPbBr_3$ nanorods (Figure S3), the synthesis details of perovskite $FA_xEA_{(1-x)}PbBr_3$ (Table S1), the summarized optical properties of perovskite $FA_xEA_{(1-x)}PbBr_3$ (Table S2), and the tolerance factor t at different doping ratio x (Table S3) (PDF)

■ AUTHOR INFORMATION

Corresponding Authors

Xiaoli Zhang − *School of Science and Engineering and Shenzhen Key Lab of Semiconductor Lasers, The Chinese University of Hong Kong, Shenzhen, Guangdong 518172, China;* orcid.org/0000-0003-1492-2068; Email: xlzhang@tju.edu.cn

Zhaoyu Zhang − *School of Science and Engineering and Shenzhen Key Lab of Semiconductor Lasers, The Chinese University of Hong Kong, Shenzhen, Guangdong 518172, China;* orcid.org/0000-0003-0335-0535; Email: zhangzy@cuhk.edu.cn

Authors

Shan Xu − *School of Science and Engineering and Shenzhen Key Lab of Semiconductor Lasers, The Chinese University of Hong Kong, Shenzhen, Guangdong 518172, China; School of Physics and Optoelectronic Engineering, Yangtze University, Jingzhou, Hubei 434023, China; Department of Optics and Optical Engineering, University of Science and Technology of China, Hefei, Anhui 230026, China;* orcid.org/0000-0003-1948-2516

Xue Ding − *School of Science and Engineering and Shenzhen Key Lab of Semiconductor Lasers, The Chinese University of Hong Kong, Shenzhen, Guangdong 518172, China*

Huafeng Shi − *Southern University of Science and Technology, Shenzhen, Guangdong 518055, China*

Xinhai Zhang − *Southern University of Science and Technology, Shenzhen, Guangdong 518055, China;* orcid.org/0000-0003-2913-1744

Xiaowei Sun − *Southern University of Science and Technology, Shenzhen, Guangdong 518055, China;* orcid.org/0000-0002-2840-1880

Ning Ji − *School of Physics and Optoelectronic Engineering, Yangtze University, Jingzhou, Hubei 434023, China*

Complete contact information is available at: https://pubs.acs.org/10.1021/acsomega.1c00213

Author Contributions

⊥S.X. and X.D. contributed equally to this work.

Notes

The authors declare no competing financial interest.

■ ACKNOWLEDGMENTS

The measurement was supported by Core Research Facilities (CRF) at SUSTech, and the authors would like to thank the engineers for their technical support. This research was supported by the Guangdong International Science and Technology Cooperation Project (no. 2019A050510002), the Shenzhen Basic Research Fund under Grant nos. JCYJ20170817112012493 and JCYJ20150929170644623, and the National Natural Science Foundation of China under Grant no. 11604026. This work is also supported by the Shenzhen Key Laboratory Project under Grant no. ZDSYS201603311644527, the President's Fund (PF01000154), the Special Fund for Applications, Science and Technology Planning Projects of Guangdong Province of China (2017B010127002), and the Open Fund of Guangdong Provincial Key Laboratory of Information Photonics Technology (Guangdong University of Technology) (no. GKPT20-09).

■ REFERENCES

(1) Baena, J. P. C.; Steier, L.; Tress, W.; Saliba, M.; Neutzner, S.; Matsui, T.; Giordano, F.; Jacobsson, T. J.; Kandada, A. R. S.; Zakeeruddin, S. M.; Petrozza, A.; Abate, A.; Nazeeruddin, M. K.; Grätzel, M.; Hagfeldt, A. Highly Efficient Planar Perovskite Solar Cells through Band Alignment Engineering. *Energy Environ. Sci.* **2015**, *8*, 2928−2934.

(2) Ma, S.; Cai, M.; Cheng, T.; Ding, X.; Shi, X.; Alsaedi, A.; Hayat, T.; Ding, Y.; Tan, Z.; Dai, S. Two-Dimensional Organic-Inorganic Hybrid Perovskite: From Material Properties to Device Applications. *Sci. China Mater.* **2018**, *61*, 1257−1277.

(3) Tan, Z.-K.; Moghaddam, R. S.; Lai, M. L.; Docampo, P.; Higler, R.; Deschler, F.; Price, M.; Sadhanala, A.; Pazos, L. M.; Credgington, D.; Hanusch, F.; Bein, T.; Snaith, H. J.; Friend, R. H. Bright Light-Emitting Diodes Based on Organometal Halide Perovskite. *Nat. Nanotechnol.* **2014**, *9*, 687−692.

(4) Xue, M.; Zhou, H.; Xu, Y.; Mei, J.; Yang, L.; Ye, C.; Zhang, J.; Wang, H. High-Performance Ultraviolet-Visible Tunable Perovskite Photodetector Based on Solar Cell Structure. *Sci. China Mater.* **2017**, *60*, 407−414.

(5) Saliba, M.; Wood, S. M.; Patel, J. B.; Nayak, P. K.; Huang, J.; Alexander-Webber, J. A.; Wenger, B.; Stranks, S. D.; Hörantner, M. T.; Wang, J. T.-W.; Nicholas, R. J.; Herz, L. M.; Johnston, M. B.; Morris, S. M.; Snaith, H. J.; Riede, M. K. Structured Organic-Inorganic Perovskite toward a Distributed Feedback Laser. *Adv. Mater.* **2016**, *28*, 923−929.

(6) Dong, R.; Fang, Y.; Chae, J.; Dai, J.; Xiao, Z.; Dong, Q.; Yuan, Y.; Centrone, A.; Zeng, X. C.; Huang, J. High-Gain and Low-Driving-Voltage Photodetectors Based on Organolead Triiodide Perovskites. *Adv. Mater.* **2015**, *27*, 1912−1918.

(7) Ding, J.; Yan, Q. Progress in Organic-Inorganic Hybrid Halide Perovskite Single Crystal: Growth Techniques and Applications. *Sci. China. Mater.* **2017**, *60*, 1063−1078.

(8) Zhang, X.; Liu, H.; Wang, W.; Zhang, J.; Xu, B.; Karen, K.; Zheng, Y.; Liu, S.; Chen, S.; Wang, K.; Sun, X. W. Hybrid Perovskite Light-Emitting Diodes Based on Perovskite Nanocrystals with Organic-Inorganic Mixed Cations. *Adv. Mater.* **2017**, *29*, 1606405−1606411.
(9) Jeon, N. J.; Noh, J. H.; Yang, W. S.; Kim, Y. C.; Ryu, S.; Seo, J.; Seok, S. I. Compositional Engineering of Perovskite Materials for High-Performance Solar Cells. *Nature* **2015**, *517*, 476−480.
(10) Cho, H.; Jeong, S.-H.; Park, M.-H.; Kim, Y.-H.; Wolf, C.; Lee, C.-L.; Heo, J. H.; Sadhanala, A.; Myoung, N.; Yoo, S.; Im, S. H.; Friend, R. H.; Lee, T.-W. Overcoming the Electroluminescence Efficiency Limitations of Perovskite Light-Emitting Diodes. *Science* **2015**, *350*, 1222−1225.
(11) Yu, J. C.; Kim, D. B.; Jung, E. D.; Lee, B. R.; Song, M. H. High-Performance Perovskite Light-Emitting Diodes Via Morphological Control of Perovskite Films. *Nanoscale* **2016**, *8*, 7036−7042.
(12) Zheng, H.; Dai, S.; Zhou, K.; Liu, G.; Zhang, B.; Alsaedi, A.; Hayat, T.; Pan, X. New-Type Highly Stable 2D/3D Perovskite Materials: The Effect of Introducing Ammonium Cation on Performance of Perovskite Solar Cells. *Sci. China Mater.* **2019**, *62*, 508−518.
(13) Yang, W. S.; Noh, J. H.; Jeon, N. J.; Kim, Y. C.; Ryu, S.; Seo, J.; Seok, S. I. High-Performance Photovoltaic Perovskite Layers Fabricated through Intramolecular Exchange. *Science* **2015**, *348*, 1234−1237.
(14) Song, J.; Li, J.; Li, X.; Xu, L.; Dong, Y.; Zeng, H. Quantum Dot Light-Emitting Diodes Based on Inorganic Perovskite Cesium Lead Halides ($CsPbX_3$). *Adv. Mater.* **2015**, *27*, 7162−7167.
(15) Zhang, A.; Lv, Q. Organic-Inorganic Hybrid Perovskite Nanomaterials: Synthesis and Application. *ChemistrySelect* **2020**, *5*, 12641−12659.
(16) Ghosh, J.; Ghosh, R.; Giri, P. K. Mesoporous Si Nanowire Templated Controlled Fabrication of Organometal Halide Perovskite Nanoparticles with High Photoluminescence Quantum Yield for Light-Emitting Applications. *ACS Appl. Nano Mater.* **2018**, *1*, 1551−1562.
(17) Schmidt, L. C.; Pertegás, A.; González-Carrero, S.; Malinkiewicz, O.; Agouram, S.; Minguez Espallargas, G.; Bolink, H. J.; Galian, R. E.; Pérez-Prieto, J. Nontemplate Synthesis of $CH_3NH_3PbBr_3$ Perovskite Nanoparticles. *J. Am. Chem. Soc.* **2014**, *136*, 850−853.
(18) Zhang, F.; Huang, S.; Wang, P.; Chen, X.; Zhao, S.; Dong, Y.; Zhong, H. Colloidal Synthesis of Air-Stable $CH_3NH_3PbI_3$ Quantum Dots by Gaining Chemical Insight into the Solvent Effects. *Chem. Mater.* **2017**, *29*, 3793−3799.
(19) Xing, J.; Liu, X. F.; Zhang, Q.; Ha, S. T.; Yuan, Y. W.; Shen, C.; Sum, T. C.; Xiong, Q. Vapor Phase Synthesis of Organometal Halide Perovskite Nanowires for Tunable Room-Temperature Nanolasers. *Nano Lett.* **2015**, *15*, 4571−4577.
(20) Oranskaia, A.; Yin, J.; Bakr, O. M.; Brédas, J.-L.; Mohammed, O. F. Halogen Migration in Hybrid Perovskites: The Organic Cation Matters. *J. Phys. Chem. Lett.* **2018**, *9*, 5474−5480.
(21) Lee, J. H.; Lee, J.-H.; Kong, E.-H.; Jang, H. M. The nature of hydrogen-bonding interaction in the prototypic hybrid halide perovskite, tetragonal $CH_3NH_3PbI_3$. *Sci. Rep.* **2016**, *6*, 21687.
(22) Tu, Y. G.; Xu, G. N.; Yang, X. Y.; Zhang, Y. F.; Li, Z. J.; Su, R.; Luo, D. Y.; Yang, W. Q.; Miao, Y.; Cai, R.; Jiang, L. H.; Du, X. W.; Yang, Y. C.; Liu, Q. S.; Gao, Y.; Zhao, S.; Huang, W.; Gong, Q. H.; Zhu, R. Mixed-cation perovskite solar cells in space. *Sci. China: Phys., Mech. Astron.* **2019**, *62*, 974221−974224.
(23) Saliba, M.; Orlandi, S.; Matsui, T.; Aghazada, S.; Cavazzini, M.; Correa-Baena, J.-P.; Gao, P.; Scopelliti, R.; Mosconi, E.; Dahmen, K.-H.; De Angelis, F.; Abate, A.; Hagfeldt, A.; Pozzi, G.; Graetzel, M.; Nazeeruddin, M. K. A molecularly engineered hole-transporting material for efficient perovskite solar cells. *Nat. Energy* **2016**, *1*, 15017.
(24) Yi, C.; Luo, J.; Meloni, S.; Boziki, A.; Ashari-Astani, N.; Grätzel, C.; Zakeeruddin, S. M.; Röthlisberger, U.; Grätzel, M. Entropic Stabilization of Mixed a-Cation ABX_3 Metal Halide Perovskites for High Performance Perovskite Solar Cells. *Energy Environ. Sci.* **2016**, *9*, 656−662.
(25) Lee, J.-W.; Kim, D.-H.; Kim, H.-S.; Seo, S.-W.; Cho, S. M.; Park, N.-G. Formamidinium and Cesium Hybridization for Photo-and Moisture-Stable Perovskite Solar Cell. *Adv. Energy Mater.* **2015**, *5*, 1501310−1501318.
(26) McMeekin, D. P.; Sadoughi, G.; Rehman, W.; Eperon, G. E.; Saliba, M.; Horantner, M. T.; Haghighirad, A.; Sakai, N.; Korte, L.; Rech, B.; Johnston, M. B.; Herz, L. M.; Snaith, H. J. A Mixed-Cation Lead Mixed-Halide Perovskite Absorber for Tandem Solar Cells. *Science* **2016**, *351*, 151−155.
(27) Hsu, H.-L.; Chang, C.-C.; Chen, C.-P.; Jiang, B.-H.; Jeng, R.-J.; Cheng, C.-H. High-Performance and High-Durability Perovskite Photovoltaic Devices Prepared Using Ethylammonium Iodide as an Additive. *J. Mater. Chem. A* **2015**, *3*, 9271−9277.
(28) Zheng, H.; Liu, G.; Chen, X.; Zhang, B.; Alsaedi, A.; Hayat, T.; Pan, X.; Dai, S. High-Performance Mixed-Dimensional Perovskite Solar Cells with Enhanced Stability against Humidity, Heat and UV Light. *J. Mater. Chem. A* **2018**, *6*, 20233−20241.
(29) Wang, Y.; Zhang, T.; Li, G.; Xu, F.; Wang, T.; Li, Y.; Yang, Y.; Zhao, Y. A Mixed-Cation Lead Iodide $Ma_{1-x}Ea_xPbI_3$ Absorber for Perovskite Solar Cells. *J. Energy Chem.* **2018**, *27*, 215−218.
(30) Liu, D.; Li, Q.; Wu, K. Ethylammonium as an Alternative Cation for Efficient Perovskite Solar Cells from First-Principles Calculations. *RSC Adv.* **2019**, *9*, 7356−7361.
(31) Dhar, A.; Dey, A.; Maiti, P.; Paul, P. K.; Roy, S.; Paul, S.; Vekariya, R. L. Fabrication and Characterization of Next Generation Nano-Structured Organo-Lead Halide-Based Perovskite Solar Cell. *Ionics* **2018**, *24*, 1227−1233.
(32) Arkan, F.; Izadyar, M. Computational Modeling of the Photovoltaic Activities in $EaBX_3$ (Ea = Ethylammonium, B = Pb, Sn, Ge, X = Cl, Br, I) Perovskite Solar Cells. *Comput. Mater. Sci.* **2018**, *152*, 324−330.
(33) Zhang, F.; Cong, J.; Li, Y.; Bergstrand, J.; Liu, H.; Cai, B.; Hajian, A.; Yao, Z.; Wang, L.; Hao, Y.; Yang, X.; Gardner, J.; Ågren, H.; Widengren, J.; Kloo, L.; Sun, L. A Facile Route to Grain Morphology Controllable Perovskite Thin Films Towards Highly Efficient Perovskite Solar Cells. *Nano Energy* **2018**, *53*, 405−414.
(34) Piccione, B.; Aspetti, C. O.; Cho, C.-H.; Agarwal, R. Tailoring light−matter coupling in semiconductor and hybrid-plasmonic nanowires. *Rep. Prog. Phys.* **2014**, *77*, 086401−086420.
(35) Lanty, G.; Bréhier, A.; Parashkov, R.; Lauret, J. S.; Deleporte, E. Strong exciton−photon coupling at room temperature in micro-cavities containing two-dimensional layered perovskite compounds. *New J. Phys.* **2008**, *10*, 065007−065017.
(36) Liao, Q.; Hu, K.; Zhang, H.; Wang, X.; Yao, J.; Fu, H. Perovskite Microdisk Microlasers Self-Assembled from Solution. *Adv. Mater.* **2015**, *27*, 3405−3410.
(37) Zhang, X.; Shi, H.; Cai, R.; Zhang, W.; Liu, H.; Yang, Y.; Sun, X. W. Formamidinium-based quasi-2D perovskite nanosheets with tunable optical properties. *IEEE Trans. Nanotechnol.* **2018**, *17*, 1165−1170.
(38) Zhu, F.; Men, L.; Guo, Y.; Zhu, Q.; Bhattacharjee, U.; Goodwin, P. M.; Petrich, J. W.; Smith, E. A.; Vela, J. Shape Evolution and Single Particle Luminescence of Organometal Halide Perovskite Nanocrystals. *ACS Nano* **2015**, *9*, 2948−2959.
(39) Imran, M.; Di Stasio, F.; Dang, Z.; Canale, C.; Khan, A. H.; Shamsi, J.; Brescia, R.; Prato, M.; Manna, L. Colloidal Synthesis of Strongly Fluorescent $CsPbBr_3$ Nanowires with Width Tunable Down to the Quantum Confinement Regime. *Chem. Mater.* **2016**, *28*, 6450−6454.
(40) Zhu, P.; Gu, S.; Shen, X.; Xu, N.; Tan, Y.; Zhuang, S.; Deng, Y.; Lu, Z.; Wang, Z.; Zhu, J. Direct Conversion of Perovskite Thin Films into Nanowires with Kinetic Control for Flexible Optoelectronic Devices. *Nano Lett.* **2016**, *16*, 871−876.
(41) Petrov, A. A.; Pellet, N.; Seo, J.-Y.; Belich, N. A.; Kovalev, D. Y.; Shevelkov, A. V.; Goodilin, E. A.; Zakeeruddin, S. M.; Tarasov, A. B.; Graetzel, M. New Insight into the Formation of Hybrid Perovskite

https://dx.doi.org/10.1021/acsomega.1c00213
ACS Omega 2021, 6, 7157−7164

Nanowires Via Structure Directing Adducts. *Chem. Mater.* **2017**, *29*, 587−594.
(42) Gu, J.; Wu, J.; Jin, C.; Sun, X.; Yin, B.; Zhang, G. C.; Wen, B.; Gao, F. Solvent Engineering for High Conversion Yields of Layered Raw Materials into Large-Scale Freestanding Hybrid Perovskite Nanowires. *Nanoscale* **2018**, *10*, 17722−17729.
(43) Pellet, N.; Gao, P.; Gregori, G.; Yang, T.-Y.; Nazeeruddin, M. K.; Maier, J.; Grätzel, M. Mixed-Organic-Cation Perovskite Photovoltaics for Enhanced Solar-Light Harvesting. *Angew. Chem., Int. Ed.* **2014**, *53*, 3151−3157.
(44) Bai, S.; Cheng, N.; Yu, Z.; Liu, P.; Wang, C.; Zhao, X.-Z. Cubic: column composite structure $(NH_2CH{=}NH_2)_x(CH_3NH_3)_{1-x}PbI_3$ for efficient hole-transport material-free and insulation layer free perovskite solar cells with high stability. *Electrochim. Acta* **2016**, *190*, 775−779.
(45) Mittal, M.; Jana, A.; Sarkar, S.; Mahadevan, P.; Sapra, S. Size of the Organic Cation Tunes the Band Gap of Colloidal Organolead Bromide Perovskite Nanocrystals. *J. Phys. Chem. Lett.* **2016**, *7*, 3270−3277.
(46) Vegard, L. Die konstitution der mischkristalle und die raumfüllung der atome. *Z. Phys.* **1921**, *5*, 17−26.
(47) Safdari, M.; Fischer, A.; Xu, B.; Kloo, L.; Gardner, J. M. Structure and function relationships in alkylammonium lead(ii) iodide solar cells. *J. Mater. Chem. A* **2015**, *3*, 9201−9207.

https://dx.doi.org/10.1021/acsomega.1c00213
ACS Omega 2021, 6, 7157−7164